

# Development of a multi-component diffusion fluid solver for a two-temperature argon plasma

Giuseppe Matteo Gangemi\*<sup>§†</sup>, Alejandro Alvarez Laguna<sup>‡</sup>, Koen Hillewaert<sup>§</sup>, Thierry Magin\*

<sup>†</sup>Corresponding author: giuseppe.gangemi@vki.ac.be

\**von Karman Institute for Fluid Dynamics*

*Waterloosesteenweg 72, 1640 Sint-Genesius-Rode (BE)*

<sup>§</sup>*Université de Liège*

*Allée de la Découverte 9, 4000 Liège (BE)*

<sup>‡</sup>*Laboratoire de Physique des Plasmas*

*CNRS, École Polytechnique, Sorbonne Université, Université Paris-Saclay*

*F-91128 Palaiseau (FR)*

## Abstract

In a wall-confined environment, the plasma behaviour can be identified by dividing the domain in two main regions: the bulk, where the quasi-neutrality prevails (the charge density is close to zero) and the sheath region near the walls, where positive space charge is built. Simulating this phenomenon poses great numerical challenges. In this work we compare results from three different approaches to numerical simulations of the plasma-sheath formation: the widely used multifluid model is presented as a referenced solution for two variations of multicomponent modeling. We present the challenges that are characteristic of each approach and propose numerical strategies to overcome them. Simulations of an isothermal binary mixture of a two-temperature argon plasma are presented at various pressure regimes.

## 1. Introduction

Accurate simulation of low temperature plasmas (i.e. plasmas with heavy temperature lower than the one of electrons) is crucial to a wide range of aerospace fields, including electronics applications (such as arcing of components used in platforms newly brought to space<sup>11</sup>), as well as hypersonics (electron transpiration cooling of innovative heat shield for cruise vehicles<sup>27</sup>). These applications vary greatly in terms of conditions (thermal non-equilibrium, pressure and so collisionality degree) and for the nature of the species involved (electrons, neutral and ionized atoms and molecules).

Huge effort has been made in the community of plasma physics in order to develop reliable simulation tools in order to join the effort of experimental science in understand the behaviour of phenomena that involves non-neutrals fluids: we are going to give here a brief review of the most relevant of these approaches (focusing on those that aim at simulating the plasma-sheath formation) but we refer the interested reader to more extensive reviews.<sup>4,8</sup>

Strategies for the numerical simulation of the plasma sheath vary depending on the collisionality of the mixture: most of the works for rarefied flows relies on kinetic approaches, like the Particle-In-Cell-Monte Carlo Collision (PIC-MCC)<sup>16</sup>; these methods provide great level of accuracy in the description of the physical phenomena but with high computational cost (with a strong direct dependency on the number of particles involved, i.e. the pressure condition). Fluid modeling represent an alternative to kinetic approaches: while describing the behaviour using macroscopic quantities reduces the accuracy and detail of the description of the gas, its computational cost is significantly reduced. Nevertheless coupling the fluid dynamics to the Maxwell's equations results in a strongly multi-scale problem that poses great challenges in the numerical development.<sup>1</sup> Some of these challenges become predominant in the development of a fluid solver that is able to simulate the interaction of plasmas with solid boundaries: a solver that describes a smooth transition from the quasi-neutral to the wall area has to respect strict constraints due to inertia disparities between electrons and heavies and has to resolve adequately the Debye length in the space charge region. Recent works have been focused on the development of asymptotic preserving schemes<sup>3,13</sup>, i.e. strategies that are able to tackle those limits in the plasma equations that introduce numerical stiffness in the simulation.

In this paper we focus on a mixture of argon, allowing to neglect for the moment complex chemical processes and to

## MULTICOMPONENT FLUID SOLVER FOR ARGON PLASMA

reduce the number of species involved.

The paper is divided as such: Section 2 introduces the governing equations for both the multifluid and the multicomponent models, detailing the scaling procedure and the main differences; Section 3 explains the numerical strategies adopted in order to retrieve the profiles shown in Sec. 4. Conclusions and possible future developments are drawn in Sec.5.

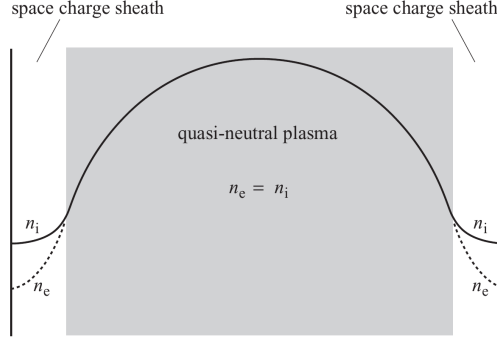


Figure 1: One dimensional discharge from Chabert & Braithwaite<sup>12</sup>.

## 2. Fluid Models

Fluid models describe the behaviour of a gas by conservation equations of macroscopic quantities derived as velocity moments of the  $k$ -th particle velocity distribution function (VDF)  $f_k(\mathbf{x}, \mathbf{c}_k, t)$ . The evolution of this quantity is accounted by means of the famous Boltzmann equation,<sup>15</sup> here we show two different scalings of it (that result in the two different models described in the next subsections):

$$\frac{\partial f_k}{\partial t} + \mathbf{c}_k \cdot \frac{\partial f_k}{\partial \mathbf{x}} + \frac{\mathbf{F}^{ext}}{m_k} \frac{\partial f_k}{\partial \mathbf{c}_k} - \sum_{k \neq j} \mathcal{J}_{kj} = \frac{1}{\text{Kn}} \mathcal{J}_{kk}, \quad \text{Multifluid} \quad (1)$$

$$\frac{\partial f_k}{\partial t} + \mathbf{c}_k \cdot \frac{\partial f_k}{\partial \mathbf{x}} + \frac{\mathbf{F}^{ext}}{m_k} \frac{\partial f_k}{\partial \mathbf{c}_k} = \frac{1}{\text{Kn}} \left( \mathcal{J}_{kk} + \sum_{j \neq k} \mathcal{J}_{kj} \right), \quad \text{Multicomponent} \quad (2)$$

where  $\mathbf{c}_k$  is the  $k$ -th particle velocity,  $\mathbf{x}$  the space coordinate,  $\mathbf{F}^{ext} = q_i(\mathbf{E} + \mathbf{c}_i \times \mathbf{B})$  are the external forces (here in the form of the Lorentz force with  $q_k$  the particle charge,  $\mathbf{E}$  the external electric field and  $\mathbf{B}$  the external magnetic field, neglected in the present tractation) and  $\mathcal{J}_{kj} = \mathcal{J}_{kj}(f_k, f_j)$  is the collision operator that describes the changes of the distribution function due to the impacts (elastic and inelastic) in the mixture. Detailed analysis of the modeling of this term is complex and beyond the scope of this document; we refer the interested reader to well-known exhaustive works.<sup>9,15</sup> As anticipated the two different treatment of the collision operator result in different macroscopic models (with  $\text{Kn}$  is the Knudsen number<sup>1</sup>): the multifluid approach distinguish the scaling of collisions between same species and between different particles, assuming that the former ones are more frequent;<sup>6</sup> the multicomponent approach on the other hand does not make this distinction (a more accurate procedure would include a sound scaling too; for such derivation we refer to Graille et al.<sup>18</sup>).

In the following subsections we detail the two main family of fluid models that result from kinetic derivation of eqs.1-2: we restrict ourselves to the case of isothermal non-equilibrium mixtures, hence the temperatures will stay constant in time and space but will be different between heavy species and electrons ( $T_h \neq T_e$ ). Such a choice has two reasons: the resulting system of equations presents already the numerical challenges that we want to tackle and, not solving the energy equation(s) allows to neglect, for the present time, the problem of closure of high order terms.<sup>28</sup>

Although these hypotheses preclude the simulation of the complete physics of many interesting phenomena, the resulting governing laws are well-suited to describe the formation of the sheath a binary mixture of argon plasma (only electrons and single-chargedly argon ions immersed in a neutral background gas composed by argon atoms) in a low-pressure discharge, as the one in Fig.1: the low pressure conditions make the energy exchange between the light electrons and heavies very inefficient (due to the low number of collisions) and so impossible to reach the thermal equilibrium.

<sup>1</sup>A more accurate definition of this parameter will be provided later in this document; here it is used to have a coherent notation with literature.

## 2.1 Multifluid models

Multifluid models represent species inside the mixture as single fluids, each one with his own dynamics: interactions between particles are accounted through source terms for collisions and external sources. We refer the interested reader to Benilov<sup>6</sup> for a complete kinetic derivation of the governing equations. From Alvarez Laguna et al.<sup>2</sup> the dimensional multifluid equations are:

$$\partial_t n_e + \partial_x (n_e u_e) = n_e \nu^{iz}, \quad (3)$$

$$\partial_t n_i + \partial_x (n_i u_i) = n_e \nu^{iz}, \quad (4)$$

$$\partial_t (n_e u_e) + \partial_x \left[ n_e u_e^2 + \frac{p_e}{m_e} \right] = -\frac{n_e q_e}{m_e} \partial_x \phi - n_e u_e \nu_{en}, \quad (5)$$

$$\partial_t (n_i u_i) + \partial_x \left[ n_i u_i^2 + \frac{p_i}{m_i} \right] = -\frac{n_i q_i}{m_i} \partial_x \phi - n_i u_i \nu_{in}, \quad (6)$$

$$\partial_{xx}^2 \phi = -\frac{(q_e n_e + q_i n_i)}{\epsilon_0}, \quad (7)$$

where  $n_k$  is the  $k$ -th species number density,  $u_k$  the  $k$ -th species velocity,  $m_k$  its mass and  $q_k$  its charge. The species partial pressure follows the perfect gas law  $p_k = n_k k_B T_k$ , with  $k_B$  the Boltzmann constant and  $T_k$  the species temperature ( $T_e$  for electrons and  $T_h$  for all the other species involved). Equation 7 is the well-known Poisson equation with  $\epsilon_0$  the vacuum permittivity and  $\phi$  the electric potential. The collision frequencies  $\nu_{en}$  and  $\nu_{in}$  account only for elastic collisions between charges and neutrals (assuming a weakly ionized plasma, i.e. a plasma where the number of charges is much lower than the neutrals):

$$\nu_{en} = \frac{16}{3} n Q_{en}^{(1,1)} \sqrt{\frac{k_B T_e}{2m_e \pi}}, \quad \nu_{in} = \frac{8}{3} n Q_{in}^{(1,1)} \sqrt{\frac{k_B T_h}{m_i \pi}}, \quad (8)$$

with  $Q_{en}^{(1,1)}$  and  $Q_{in}^{(1,1)}$  collision integrals<sup>22</sup> dependent on temperature and obtained from the thermodynamic library Mutation++<sup>26</sup>. The dynamics of neutral background gas is not simulated and assumed at rest (the collisional terms in eqs.5-6 simplify to  $n_k (u_k - u_n) \nu_{kn} = n_k u_k \nu_{kn}$ ).

Equations 3-7 can be rescaled introducing appropriate reference quantities:

$$\bar{x} = x/L_0, \quad \bar{u}_k = u_k/u_0, \quad \bar{t} = t/t_0, \quad \bar{n} = n/n_0, \quad \bar{\phi} = \phi/\phi_0, \quad \bar{\nu}^{iz} = \nu^{iz} t_0, \quad (9)$$

where  $L_0 = L$  is the domain length,  $u_0 = u_B = \sqrt{k_B T_e / m_i}$  is the Bohm velocity and the reference timescale is obtained as  $t_0 = L_0 / u_0$ ;  $n_0 = n_{e0}$  is the initial electron number density and the reference potential is defined as  $\phi_0 = k_B T_e / e$  (the electron temperature in eV). Elastic collision frequencies requires a special treatment: we start by scaling with the reference velocity

$$\nu_{en} = \frac{16}{3\sqrt{2\pi}} \frac{1}{\sqrt{\epsilon}} n Q_{en}^{(1,1)} [u_0], \quad \nu_{in} = \frac{8\sqrt{\kappa}}{3\sqrt{\pi}} n Q_{in}^{(1,1)} [u_0]. \quad (10)$$

Few passages allow to obtain expressions that are dependent on the Knudsen number  $\text{Kn}_{kn} = \lambda_{kn} / L_0$  (with  $\lambda_{kn} = (n Q_{kn}^{(1,1)})^{-1}$  the mean free path for the collision between particle  $k$  and a neutral atom):

$$\nu_{en} = \frac{16}{3\sqrt{2\pi}} \frac{1}{\sqrt{\epsilon}} \underbrace{n Q_{en}^{(1,1)} L_0}_{\text{Kn}_{en}^{-1}} \underbrace{\left[ \frac{u_0}{L_0} \right]}_{t_0^{-1}}, \quad \nu_{in} = \frac{8}{3\sqrt{\pi}} \sqrt{\kappa} \underbrace{n Q_{in}^{(1,1)} L_0}_{\text{Kn}_{in}^{-1}} \underbrace{\left[ \frac{u_0}{L_0} \right]}_{t_0^{-1}}. \quad (11)$$

The final scaled form for the multifluid model is then obtained:

$$\partial_{\bar{t}} \bar{n}_e + \partial_{\bar{x}} (\bar{n}_e \bar{u}_e) = \bar{n}_e \bar{\nu}^{iz}, \quad (12)$$

$$\partial_{\bar{t}} \bar{n}_i + \partial_{\bar{x}} (\bar{n}_i \bar{u}_i) = \bar{n}_e \bar{\nu}^{iz}, \quad (13)$$

$$\partial_{\bar{t}} (\bar{n}_e \bar{u}_e) + \partial_{\bar{x}} \left[ \bar{n}_e (\bar{u}_e^2 + \epsilon^{-1}) \right] = \epsilon^{-1} \bar{n}_e \partial_{\bar{x}} \bar{\phi} - \bar{n}_e \bar{u}_e \left( \frac{16}{3\sqrt{2\pi}} \frac{1}{\sqrt{\epsilon} \text{Kn}_{en}} \right), \quad (14)$$

$$\partial_{\bar{t}} (\bar{n}_i \bar{u}_i) + \partial_{\bar{x}} \left[ \bar{n}_i (\bar{u}_i^2 + \kappa) \right] = -\bar{n}_i \partial_{\bar{x}} \bar{\phi} - \bar{n}_i \bar{u}_i \left( \frac{8}{3\sqrt{\pi}} \frac{\sqrt{\kappa}}{\text{Kn}_{in}} \right), \quad (15)$$

$$\partial_{\bar{x}\bar{x}}^2 \bar{\phi} = \chi^{-1} (\bar{n}_e - \bar{n}_i), \quad (16)$$

## MULTICOMPONENT FLUID SOLVER FOR ARGON PLASMA

Equations<sup>2</sup> 12-16 present different adimensional parameters: these, together with relevant quantities for the testcase in object, are shown in Tab.1 .

Table 1: Argon discharge conditions

Initial electron number density	$n_{e0}$	$10^{16} \text{ m}^{-3}$	Heavy temperature	$T_h$	0.05 eV
Electron Temperature	$T_e$	2 eV	Ion-neutral collision integral	$Q_{in}^{(1,1)}$	$1.41 \times 10^{-18} \text{ m}^2$
Electron-neutral collision integral	$Q_{en}^{(1,1)}$	$7 \times 10^{-20} \text{ m}^2$	Electron-to-ion mass ratio	$\varepsilon = m_e/m_i$	$1.36 \times 10^{-5}$
Ion-to-electron temperature ratio	$\kappa = T_h/T_e$	0.025	Initial Debye length	$\lambda_D$	$10^{-4} \text{ m}$
Electron plasma period	$\omega_{pe}^{-1}$	$1.77 \times 10^{-10} \text{ s}$	Discharge width	$L$	$100 \lambda_D$

Equations 12-15 represent the fluid dynamic subset, with density conservation equations for each species (eqs.12,13) and their momentum conservation equations (eqs.14,15) We consider only ionization processes ( $\nu^{iz}$ ) as source term for the density conservation equations; the ionization frequency  $\nu^{iz}$  is an eigenvalue of the problem<sup>25</sup> so we implement here the iterative formula already detailed in previous works<sup>2,3</sup> :

$$\nu^{iz} = \frac{|(n_i u_i)^L + (n_i u_i)^R|}{\int_L n_e(X) dx}, \quad (17)$$

where subscripts  $L, R$  indicate, respectively, left and right wall. The ionization frequency is calculated in order to replenish the domain with the same number of particles that leaves the domain and in order to keep the number of electrons inside the discharge constant.

### 2.1.1 Boundary conditions

The multifluid equations present an hyperbolic scaling so the quantities to be (or not to be) imposed at the interface have to be chosen accordingly: following Alvarez Laguna et al.<sup>3</sup> we impose the electron flux to both boundaries to be equal to the number of particles crossing the plane with positive velocity component (assuming a maxwellian VDF). In normalized quantities:

$$\Gamma_e^{L,R} = (n_e u_e)^{L,R} = \mp \frac{n_e}{\sqrt{2\pi\varepsilon}}. \quad (18)$$

Electron density has Neumann boundary on both sides; ion quantities (density and momentum) have the same Neumann condition, as the flux of positive charges arriving at the wall is assumed supersonic. The electric potential is imposed on both sides  $\phi(x = \{0, L\}, t) = 0$  but can be easily be biased to different values.

### 2.2 Multicomponent models

We show in this section the governing equations under the multicomponent modeling<sup>17</sup> assumption. In this case the plasma is considered a single fluid with the different species diffusing inside it:

$$\partial_t n_e + \partial_x (n_e u) + \partial_x (n_e V_e) = n_e \nu^{iz}, \quad (19)$$

$$\partial_t n_i + \partial_x (n_i u) + \partial_x (n_i V_i) = n_e \nu^{iz}, \quad (20)$$

$$\partial_t (\rho u) + \partial_x (\rho u^2 + p) = \partial_x \Pi - nq \partial_x \phi, \quad (21)$$

$$\partial_{xx}^2 \phi = \chi^{-1} (n_e - n_i), \quad (22)$$

where  $u$  is the velocity of the entire fluid,  $V_k$  is the diffusion velocity of the  $k$ -th species,  $p = \sum_{j \in S} p_j$  the total pressure and  $\Pi$  the stress tensor. The one dimensional discharge chosen as testcase of this work can be modeled as a pure diffusion problem; therefore assuming  $u = 0$  we can get rid of eq.21 and of the convective terms in eqs.19, 20:

$$\partial_t n_e + \partial_x (n_e V_e) = n_e \nu^{iz}, \quad (23)$$

$$\partial_t n_i + \partial_x (n_i V_i) = n_e \nu^{iz}, \quad (24)$$

$$\partial_{xx}^2 \phi = \chi^{-1} (n_e - n_i), \quad (25)$$

<sup>2</sup>The notation  $(\bar{\cdot})$  will be abandoned in the rest of the document for the sake of clarity, but quantities will be considered scaled (unless differently specified).

The source term for eqs.23-24 is calculated using eq.17, using in this case only the ion diffusive flux  $(n_i V_i)^{L,R}$  to the wall instead of  $(n_i u_i)^{L,R}$ .

Different approaches exist for the modeling of the diffusion velocity; in this document we present the binary diffusion (here referred to with "BD") model and the multicomponent diffusion (referred here later as "MC" or "MC Diffusion") model. The former is simpler and is modeled on the classic drift-diffusion equations<sup>7</sup> :

$$V_k = \left( -\frac{D_k}{n_k} \partial_x n_k - \mu_k \partial_x \phi \right) \quad (26)$$

with species diffusion coefficient  $D_k$  and the species mobility  $\mu_k$  (adapted for charges-neutral collisions):

$$D_k = \frac{k_B T_k}{m_k \nu_{kn}}, \quad \mu_k = \frac{q_k}{m_k \nu_{kn}}. \quad (27)$$

As the name suggests the model takes into account only binary interactions, losing its accuracy when the mixture contains more than one species. Such inconvenient is overcome by the slightly more complex multicomponent diffusion approach<sup>21</sup> (adapted under the isothermal assumption):

$$V_k = - \sum_{j \in \mathcal{S}} \mathcal{D}_{kj} \left[ \frac{T_j}{T_h} \frac{\partial_x n_j}{n} - y_j \sum_{m \in \mathcal{S}} \frac{T_m}{T_h} \frac{\partial_x n_m}{n} + \frac{(x_j q_j - y_j Q)}{k_B T_h} \partial_x \phi \right], \quad k \in \mathcal{S} \quad (28)$$

where  $\mathbf{D} = [\mathcal{D}_{kj}]$  is the multicomponent diffusion matrix, here computed using Ramshaw approach,<sup>24</sup>  $x_j$  and  $y_j$  are, respectively, the molar and mass fraction and  $Q = \sum_{m \in \mathcal{S}} x_m q_m$  is the mixture charge. Coefficients in the multicomponent diffusion matrix are obtained using the thermodynamic library Mutation++. The multicomponent diffusion model allows to couple the diffusion of all the particles at the same time: in order to retrieve a similar behaviour to the one produced by the multifluid equations, we set the neutral properties at the starting condition and we keep them constant in time, obtaining accordingly the transport properties for the entire mixture; the dynamics of the neutrals atoms is then considered negligible, due to the assumed low ionization degree. As already mentioned, a rigorous kinetic derivation of the multicomponent equations can be found in Graille et al.<sup>18</sup>

In the case of a binary mixture (like the one treated here) the multicomponent diffusion should degenerate in the binary diffusion: we will see the comparison of the two assumptions in the dedicated section.

We will not repeat here all the passages detailed in the previous section to obtain scaled equations and we will limit ourselves to present the final version of the diffusion velocities here:

$$V_e^{\text{BD}} = \frac{3\sqrt{2\pi}}{16} \frac{\text{Kn}_{en}}{\sqrt{\varepsilon}} \left( -\frac{\partial_x n_e}{n_e} + \partial_x \phi \right), \quad V_i^{\text{BD}} = \frac{3\sqrt{\pi}}{8} \frac{\text{Kn}_{in}}{\sqrt{\kappa}} \left( -\frac{\kappa \partial_x n_i}{n_i} - \partial_x \phi \right) \quad (29)$$

$$V_k^{\text{MC}} = - \sum_{j \in \mathcal{S}} \bar{\mathcal{D}}_{kj} \left[ \frac{T_j}{T_h} \frac{\partial_x n_j}{n} - y_j \sum_{m \in \mathcal{S}} \frac{T_m}{T_h} \frac{\partial_x n_m}{n} + (x_j q_j - y_j Q) \partial_x \phi \frac{T_e}{T_h} \right]. \quad (30)$$

Coefficients in  $\bar{\mathcal{D}}_{kj}$  depend on the Knudsen number in a similar way to the adimensional collisional frequencies:

$$\bar{\mathbf{D}} = \bar{\mathcal{D}}_{kj} = \begin{bmatrix} \bar{\mathcal{D}}_{ee} & \bar{\mathcal{D}}_{ei} & \bar{\mathcal{D}}_{en} \\ \bar{\mathcal{D}}_{ie} & \bar{\mathcal{D}}_{ii} & \bar{\mathcal{D}}_{in} \\ \bar{\mathcal{D}}_{ne} & \bar{\mathcal{D}}_{ni} & \bar{\mathcal{D}}_{nn} \end{bmatrix}, \quad \bar{\mathcal{D}}_{kj} = \frac{(\delta_{kj} - y_j)(1 - y_j)}{x_j(1 - x_j)} \tilde{\mathcal{D}}_j \quad (31)$$

where  $\delta_{ij}$  is Kronecker's delta and  $\tilde{\mathcal{D}}_j$  is the effective binary diffusivity for species  $j$ :

$$\tilde{\mathcal{D}}_k = (1 - x_k) \left( \sum_{j \neq i} \frac{x_j}{\mathcal{D}_{kj}} \right)^{-1} \quad \mathcal{D}_{kj} = \begin{cases} \mathcal{D}_{kj} = \frac{3}{8} \sqrt{\pi \kappa} \text{Kn}_{kj} L_0 & k, j \in \mathcal{H} \\ \mathcal{D}_{ie} = \frac{3}{16} \sqrt{\frac{2\pi}{\varepsilon}} \text{Kn}_{ke} L_0 & k \in \mathcal{H} \\ \mathcal{D}_{ee} = \frac{3}{8} \sqrt{\frac{\pi}{\varepsilon}} \text{Kn}_{ee} L_0 & \end{cases} \quad (32)$$

with  $\mathcal{H} = \mathcal{S} - \{e\}$  the heavy subset. In the previous equations we assumed  $m_n \sim m_i$ , choice justified if we consider a mixture where the neutral species is the *parent* atom of the ion ( $m_n = m_i + m_e$ ); the case of more complex mixtures is left for future developments.

The multicomponent diffusion naturally takes into account the interactions between all the particles in the mixtures (some of which we neglected in the binary diffusion or multifluid approach): those that do not involve neutrals have reduced impact on the solution due to the low ionization degree of the mixtures investigated ( $x_e \sim x_i \ll x_n$  and  $y_e \ll y_i \ll y_n$ ).

## MULTICOMPONENT FLUID SOLVER FOR ARGON PLASMA

**2.2.1 Boundary conditions**

Setting the boundary conditions to the multicomponent modeling presents substantial differences with respect to the multifluid counterpart. Equations 23, 24 present a typical elliptic scaling: following the approach in Hagelaar<sup>19</sup> (but common in literature, see for example Artola et al.<sup>5</sup>) we impose Neumann boundary conditions both on electrons and ions. The diffusion flux to the wall of these species is defined as:

$$\Gamma_e^{L,R} = (n_e V_e)^{L,R} = \mp \frac{n_e}{\sqrt{2\pi\epsilon}}, \quad (33)$$

$$\Gamma_i^{L,R} = (n_i V_i)^{L,R} = \mp n_i \sqrt{\frac{\kappa}{2\pi}} + \Gamma_i^\phi, \quad (34)$$

where the additional flux to the wall

$$\Gamma_i^{\phi, \text{BD}} = -\frac{n_i}{v_{in}} \partial_x \phi \quad (35)$$

$$\Gamma_i^{\phi, \text{MC}} = n_i \left( -\sum_{j \in \mathcal{S}} \bar{\mathcal{D}}_{kj} (x_j q_j - y_j \mathcal{Q}) \partial_x \phi \frac{T_e}{T_h} \right) \quad (36)$$

is imposed in order to prevent numerical accumulation of ions at the wall. The boundary condition of the electric potential remains unchanged and has been detailed in Section 2.1.1.

**3. Numerical strategies**

In order to detail the numerical methods employed here, we are going to rewrite eqs.12-16 and eqs.23-25 as:

$$\partial_t \mathbf{U} + \partial_x \mathbf{F}(\mathbf{U}) = \mathbf{S}(\mathbf{U}), \quad (37)$$

with:

$$\mathbf{U}^{\text{MF}} = \begin{bmatrix} n_e \\ n_i \\ n_e u_e \\ n_i u_i \\ \phi \end{bmatrix} \quad \mathbf{U}^{\text{BD}} = \begin{bmatrix} n_e \\ n_i \end{bmatrix} \quad \mathbf{U}^{\text{MC}} = \begin{bmatrix} n_e \\ n_i \\ \phi \end{bmatrix} \quad (38)$$

and:

$$\mathbf{F}^{\text{MF}} = \begin{bmatrix} n_e u_e \\ n_i u_i \\ n_e (u_e^2 + \epsilon^{-1}) \\ n_i (u_i^2 + \kappa) \\ \partial_x \phi \end{bmatrix} \quad \mathbf{F}^{\text{BD}} = \begin{bmatrix} n_e V_e \\ n_i V_i \end{bmatrix} \quad \mathbf{F}^{\text{MC}} = \begin{bmatrix} n_e V_e \\ n_i V_i \\ \partial_x \phi \end{bmatrix} \quad (39)$$

$$\mathbf{S}^{\text{MF}} = \begin{bmatrix} n_e v^{iz} \\ n_e v^{iz} \\ \epsilon^{-1} n_e \partial_x \phi - n_e u_e v_{en} \\ -n_i \partial_x \phi - n_i u_i v_{in} \\ \chi^{-1} (n_e - n_i) \end{bmatrix} \quad \mathbf{S}^{\text{BD}} = \begin{bmatrix} n_e v^{iz} \\ n_e v^{iz} \end{bmatrix} \quad \mathbf{S}^{\text{MC}} = \begin{bmatrix} n_e v^{iz} \\ n_e v^{iz} \\ \chi^{-1} (n_e - n_i) \end{bmatrix} \quad (40)$$

The use of indices <sup>MF</sup>, <sup>BD</sup> and <sup>MC</sup> will be omitted (when not needed) in the rest of the document for the seek of clarity. We do not describe the details of the space discretization for all the schemes proposed when their use is wide known and not different from the applications in classic fluid dynamics; on the other hand, next section contains the description of the time integration schemes used, as their choice is fundamental in the development of the solvers.

**3.1 Multifluid**

The multifluid model is the most common in the plasma physics community and it has been used extensively to simulate the plasma-sheath formation. For this reason we choose as reference solutions the one obtained using Finite Volumes, with explicit third order Runge-Kutta and Roe numerical flux with third order reconstruction of the solution<sup>10</sup>; the electric potential is obtained by solving the Poisson equation at any timestep using centered finite differences. The

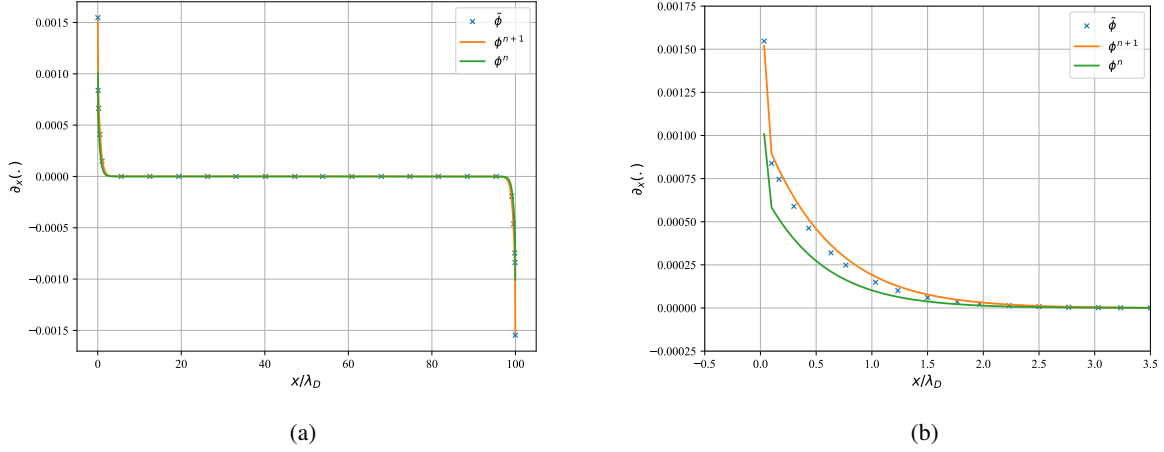


Figure 2: Gradient of the electric potential  $\phi$  evaluated at timestep  $\{n, n + 1\}$  and the predicted value obtained with eq.43. Values obtained at the first steps of the simulation.

electron plasma frequency imposes strict constraints for explicit schemes but this does not impact too heavily the computational cost of the simulation. This consideration is not valid for multicomponent schemes where the presence of diffusive terms is well-known source of numerical stiffness: for this reason the next two section will show semi-implicit and implicit time integration schemes.

### 3.2 Binary diffusion

A first order backward Euler has been implemented in order to solve for eqs.23-25: the simplicity of this solution reflects the simplicity of the modeling. As already mentioned the binary diffusion model coincides with multicomponent diffusion approach when the mixture accounts only for binary interactions: we choose here to present it as a further test for the implementation of the more complete approach.

We focus here on the electron diffusion flux, rewriting it in non-conservative form<sup>3</sup> (but the same reasoning can be applied on the other species):

$$\partial_x \left( -\partial_x n_e^{n+1} + n_e^{n+1} \partial_x \tilde{\phi} \right) = - \left( \partial_{xx}^2 n_e \right)^{n+1} + (\partial_x n_e)^{n+1} (\partial_x \tilde{\phi}) + (n_e)^{n+1} (\partial_{xx}^2 \tilde{\phi}), \quad (41)$$

In this way the expression is linear with the number density and so the system of equations:

$$\left( \frac{\mathbf{I}}{\Delta t} + \mathbf{A}_j^{\text{BD},n} \right) \mathbf{U}^{\text{BD},n+1} = \frac{\mathbf{I}}{\Delta t} \mathbf{U}^{\text{BD},n} + \mathbf{S}^{\text{BD},n}. \quad (42)$$

is tridiagonal ( $\mathbf{A}_j^{\text{BD},n}$  is the matrix resulting from discretizing eq.41 using centered finite differences) and can be solved using the fast Thomas algorithm. In eq.41 the derivatives of the potential  $\phi$  are not evaluated at  $t = n + 1$ , which will require to solve the Poisson equation coupled to the system, but instead a *prediction* of the value  $\tilde{\phi}$  is used; this allows to obtain greater stability without increasing excessively the computational cost. The predicted value of the electric potential is obtained solving:

$$-\partial_x \left[ \left( \chi - \Delta t \sum_{j \in \mathcal{S}} |q_j| \frac{n_j^n}{v_{jn}} \right) \partial_x \tilde{\phi} \right] = \sum_{j \in \mathcal{S}} q_j (2n_j^n - n_j^{n-1}) + \Delta t \partial_x \left( |q_j| \frac{n_j^k}{v_{jn}} \partial_x \phi^n \right). \quad (43)$$

The steps to obtain the previous equation are detailed in Hagelaar<sup>19</sup> and have been adapted to our governing laws. The electric potential  $\tilde{\phi}$  can be obtained using centered finite differences and solving the resulting tridiagonal system using the Thomas algorithm. Figure 2 shows the quality of this method: the procedure is able to give a satisfying prediction of the value, improving the stability of the scheme (for a more detailed description of the properties of the scheme see Bessemoulin-Chatard et al.<sup>7</sup>).

<sup>3</sup>Indices  $\{n + 1, n, n - 1\}$  indicate the timestep at which the considered quantity is evaluated.

## MULTICOMPONENT FLUID SOLVER FOR ARGON PLASMA

**3.3 Multicomponent diffusion**

For the multicomponent diffusion approach we follow Munafó<sup>23</sup> and Hirsch<sup>20</sup> in order to obtain a second order implicit formula (Backward Differentiation Formula - BDF2). We rewrite eqs.37 as:

$$\alpha \partial_t \mathbf{U} + \partial_x \mathbf{F}(\mathbf{U}^{n+1}) - \mathbf{S}(\mathbf{U}^{n+1}) = 0, \quad \alpha = \begin{cases} 1 & \text{Fluid Equations} \\ 0 & \text{Poisson} \end{cases} \quad (44)$$

and discretized according to the classical Finite Volumes method:

$$\alpha \frac{\partial \mathbf{U}_i}{\partial t} \Delta x_i + \mathbf{F}_{i+\frac{1}{2}}^{n+1} - \mathbf{F}_{i-\frac{1}{2}}^{n+1} - \mathbf{S}_i^{n+1} \Delta x_i = 0. \quad (45)$$

We define the pseudo-steady residual array:

$$\mathbf{H}(\mathbf{U}) = \alpha \frac{\partial \mathbf{U}}{\partial t} \Delta x_i + \mathbf{R}(\mathbf{U}) = 0, \quad \mathbf{R}(\mathbf{U}) = \mathbf{F}_{i+\frac{1}{2}} - \mathbf{F}_{i-\frac{1}{2}} - \mathbf{S} \Delta x_i \quad (46)$$

and employ a three-point Backward Euler schemes:

$$\mathbf{H}(\mathbf{U}) = \alpha \frac{3\mathbf{U}^{k+1} - 4\mathbf{U}^k + \mathbf{U}^{k-1}}{2\Delta t} \Delta x_i + \mathbf{R} = 0 \quad (47)$$

The jacobian matrix:

$$\frac{\partial \mathbf{H}}{\partial \mathbf{U}} = \alpha \frac{3}{2\Delta t} \Delta x_i + \frac{\partial \mathbf{R}}{\partial \mathbf{U}}$$

is calculated analytically through linearization of terms in eq.45. The diffusion term is given by:

$$\mathbf{F}_{i+\frac{1}{2}}^n = \mathbf{A}_{i+\frac{1}{2}}^n \left( \frac{\partial \mathbf{U}}{\partial x} \right)_{i+\frac{1}{2}} \quad (48)$$

where the matrix is:

$$\mathbf{A}_{i+\frac{1}{2}} = \begin{bmatrix} \mathbf{A}_{N_S \times N_S}^{f,f} & \mathbf{A}_{N_S \times 1}^{f,\phi} \\ \mathbf{0}_{1 \times N_S} & 1 \end{bmatrix} \quad (49)$$

The block  $\mathbf{A}_{N_S \times N_S}^{f,f}$  accounts for the dependency of the flux in eq.23-24 with respect to the  $f$  (fluid) variables while the block  $\mathbf{A}_{N_S \times 1}^{f,\phi}$  accounts for the dependency with respect to the electric potential  $\phi$ . The bottom part results from the simple consideration  $\partial_{xx}^2 \phi = \partial_x (\partial_x \phi)$  and acknowledging that there is no dependency on the gradient of the fluid variables.

The block matrices are defined as (in their scaled form):

$$\mathbf{A}_{N_S \times N_S}^{f,f} = [\mathcal{A}_{ij}], \quad \mathcal{A}_{ij} = -\frac{n_i}{n} \left[ \sum_{m \in \mathcal{S}} (\delta_{jm} - y_m) \mathcal{D}_{im} \right] \frac{T_j}{T_h} \quad i, j \in \mathcal{S} \quad (50)$$

$$\mathbf{A}_{N_S \times 1}^{f,\phi} = [\mathcal{A}_i], \quad \mathcal{A}_i = -\frac{n_i}{n} \left[ \sum_{j \in \mathcal{S}} \mathcal{D}_{ij} (n_j q_j - y_j Q) \right] \frac{T_e}{T_h}, \quad Q = \sum_{m \in \mathcal{S}} n_m q_m \quad (51)$$

The expressions obtained are then linearized around the time-level  $n$  as follows:

$$\mathbf{F}_{i+\frac{1}{2}}^{n+1} \simeq \mathbf{F}_{i+\frac{1}{2}}^n + 2\mathbf{A}_{i+\frac{1}{2}}^n \left( \frac{\mathbf{U}_{i+1}^n - \mathbf{U}_i^n}{\Delta x_{i+1} + \Delta x_i} \right), \quad (52)$$

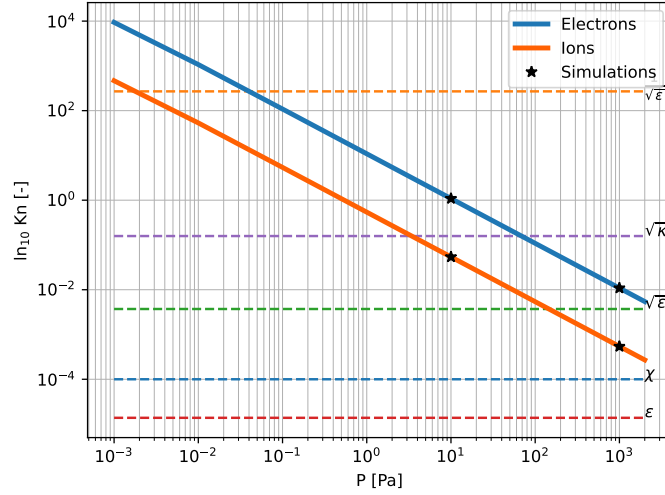
with  $\Delta x_{i+1}, \Delta x_i$  being the dimension of, respectively, cell  $i+1$  and  $i$ . The source term  $\mathbf{S}^{n+1}$  is taken as

$$\mathbf{S}_i^{n+1} = [n_e v^{iz}]_i^{n+1} \simeq [n_e]_i^{n+1} (v^{iz})^n \quad (53)$$

assuming the ionization frequency as constant in time: this results in a simplified jacobian  $\partial \mathbf{S} / \partial \mathbf{U}$  that does not break the sparseness of the matrix.

The complete system (47) is approximated then by solving the linear system:

$$\left( \frac{\partial \mathbf{H}}{\partial \mathbf{U}} \right) \mathbf{U}^{n+1} = \mathbf{M}_{Li}^n \mathbf{U}_{i-1}^{n+1} + \mathbf{M}_{Ci}^n \mathbf{U}_i^{n+1} + \mathbf{M}_{Ri}^n \mathbf{U}_{i+1}^{n+1} = -\mathbf{R}_i \quad (54)$$

Figure 3: Knudsen number at different pressures ( $L_0 = L$ ) with the results conditions highlighted.

with each term calculated as follows:

$$\mathbf{M}_{Li} = \frac{2\mathbf{A}_{i-1/2}}{(\Delta x_i + \Delta x_{i-1})} \quad (55a)$$

$$\mathbf{M}_{Ci} = \left[ \alpha \frac{3}{2\Delta t} - \frac{\partial \mathbf{S}}{\partial \mathbf{U}} \right] \Delta x_i - \frac{2\mathbf{A}_{i-1/2}}{(\Delta x_i + \Delta x_{i-1})} - \frac{2\mathbf{A}_{i+1/2}}{(\Delta x_{i+1} + \Delta x_i)} \quad (55b)$$

$$\mathbf{M}_{Ri} = \frac{2\mathbf{A}_{i+1/2}}{(\Delta x_{i+1} + \Delta x_i)} \quad (55c)$$

$$\mathbf{R}_i = \alpha \frac{(-4\mathbf{U}^n + \mathbf{U}^{n-1})}{2\Delta t} \Delta x_i + \mathbf{F}_{i+\frac{1}{2}}^n - \mathbf{F}_{i-\frac{1}{2}}^n - \mathbf{S}_i^n \quad (55d)$$

Iterations are performed using a Newton solver until  $\|\mathbf{U}^{n+1} - \mathbf{U}^n\| < 10^{-8}$ .

Table 2: Simulation conditions

	$p_n$	$n_n$	$\eta = \frac{n_{e0}}{n_n}$	$\text{Kn}_{en}$	$\text{Kn}_m$
Low Pressure	10 Pa	$1.25 \times 10^{21} \text{ m}^{-3}$	$\sim 10^{-5}$	1.088	0.054
High Pressure	1000 Pa	$1.25 \times 10^{23} \text{ m}^{-3}$	$\sim 10^{-7}$	0.0108	$5.4 \times 10^{-4}$

## 4. Results

We proceed here to show the results of the simulations for different levels of pressure in order to investigate various collisional regimes. In Fig.3 we show how the Knudsen number:

$$\text{Kn}_{kn} = \frac{\lambda_{kn}}{L_0} = \frac{1}{nQ_{kn}^{(1,1)}L_0} \quad (56)$$

varies with pressure. The number density  $n$  of the mixture is chose as  $n \sim n_n = p_n / (k_B T_h)$  given the low ionization degree that we want to maintain. In this sense the reference number density is kept constant ( $n_0 = n_{e0} = 10^{16} \text{ m}^{-3}$ ) and only the background gas pressure is modified: Table 2 details the condition of the two regimes we are showing here, one for the low pressure and one for the high pressure.

We compare solutions from the multifluid, binary diffusion and multicomponent diffusion models in terms of number density, (diffusion) velocity and electric potential profiles. The velocity values have been scaled first with a common

## MULTICOMPONENT FLUID SOLVER FOR ARGON PLASMA

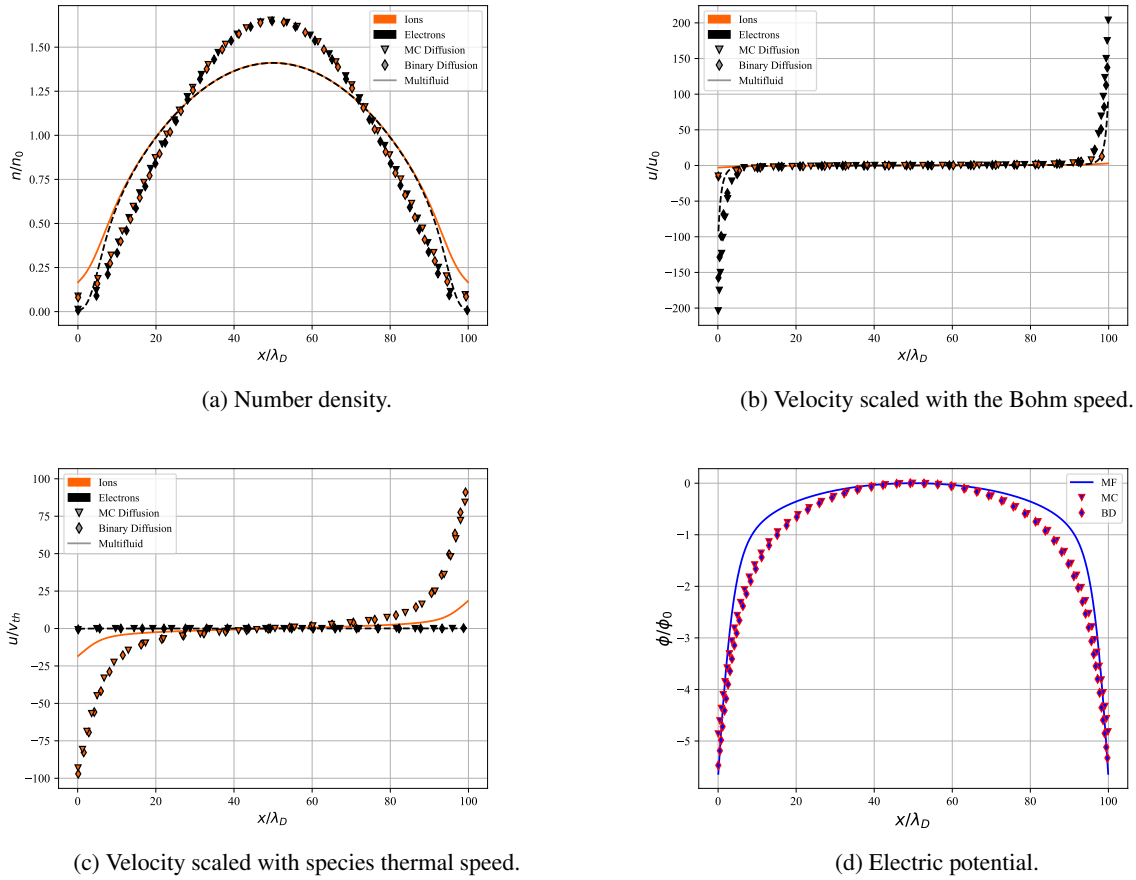


Figure 4: Low pressure (10 Pa) solution for the multifluid, binary diffusion and multicomponent diffusion models.

value (the classical Bohm speed), in order to emphasize the different magnitude between the two species, and with a species-specific value (its thermal velocity):

$$v_{th,k} = \sqrt{\frac{8k_B T_k}{\pi m_k}}. \quad (57)$$

This last choice allows to clearly show how the ions reach highly supersonic regimes in contrast with electrons: the sheath dimension is too small to allow the potential drop to accelerate the particles to their high speed of sound. All the computations are advanced until a steady state solution is reached.

#### 4.1 Low Pressure

For the low pressure case we choose to perform simulation at 10 Pa and the results are shown in Fig.4-5. As we see all the approaches are able to capture both the quasineutral and charged region but we clearly see how the overall general agreement is poor throughout the entire domain: in particular the multifluid and both multicomponent model reach different value of number density in the center of the bulk region as well as in the regions close to the walls. As from eq.17, the steady state value of the ionization is directly linked to the boundary condition imposed at the wall: the boundary conditions differ greatly between the two models and at this level of pressure they may not give the same wall flux (Fig.5a). Accordingly fig.4b-4c show great mismatch comparing particle velocities and particle diffusion velocities: approaching the wall (Fig.5b-5c) the multicomponent models greatly overestimate the speed with which the species leave the domain influencing both the solution in the sheath and, as already highlighted, the value in the bulk. It is worth to mention that in the collisionless limit fluid models, even though numerically possible, loses their fundamental assumption (the continuum regime or  $Kn \ll 1$ ): However, previous works<sup>2</sup> demonstrated that fluid governing laws can compare well with particle methods even in the rarefied regime, hence the interest of this work in the investigation of the limits of the novel proposed multicomponent approach.

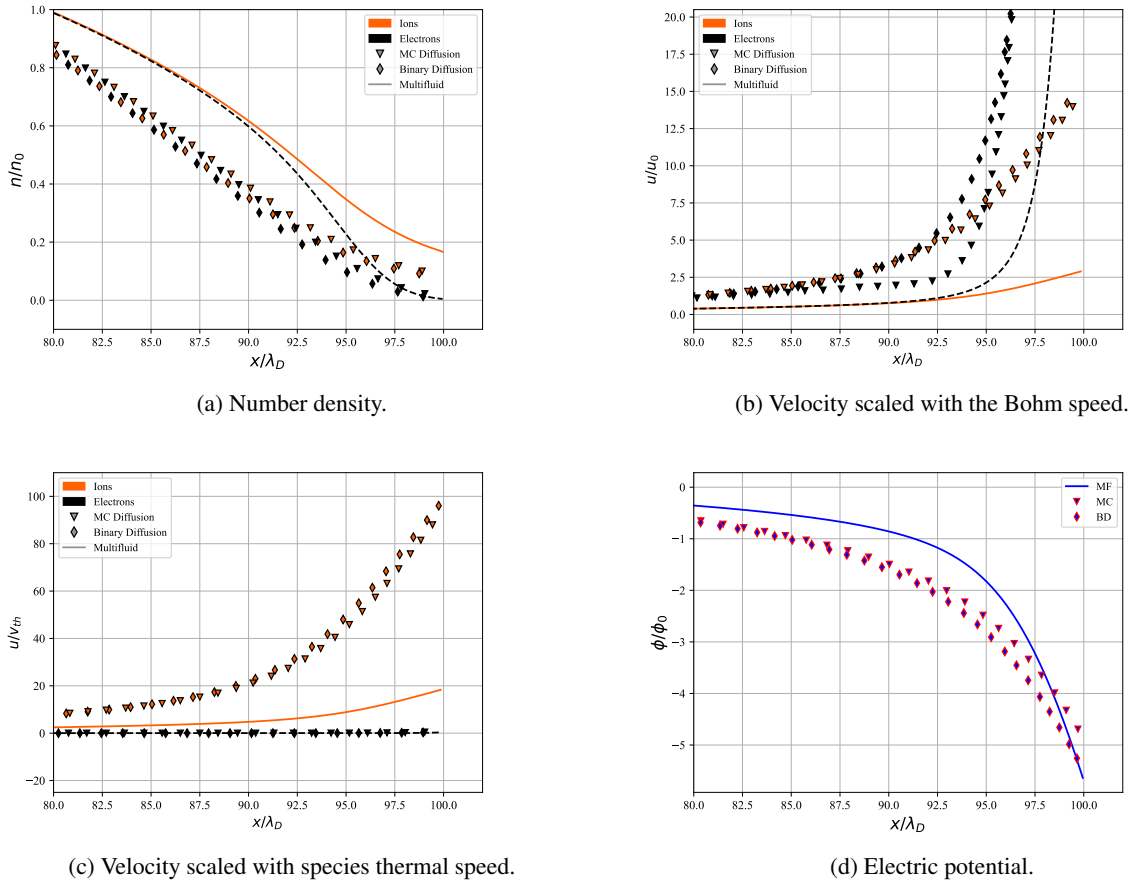


Figure 5: Low pressure (10 Pa) solution for the multifluid, binary diffusion and multicomponent diffusion models (Particular of the sheath region).

## 4.2 High Pressure

The high pressure regime has been investigated by setting  $p_n = 1000$  Pa: the higher collisional regime directly reflects into a greater agreement in all the quantities shown (Fig.6-7).

The number densities computed with the different approaches show the same profile both in the center of the domain and in the sheath (Fig.7a): we see that imposing different boundary conditions do not impact significantly the result. In the proximity of the wall (Fig.7a), the multicomponent models are able to capture correctly the value produced by the reference solution.

The increased number of collisions can be seen in the reduced velocity of particles entering the sheath (compare in this sense Fig.5b-5c with Fig.7b-7c); at higher pressure the effect of collisions reduces the importance of inertial terms leading the multifluid model towards a diffusive limit that well agrees with the multicomponent approach. In addition, this might suggest that the purely diffusive hypothesis made in Sec.2.2 might not be valid when the number of collisions is not high enough. We reserve these investigations for future developments.

Figure 7b show profile that might seem to contradict the theory: indeed all models predict ion speed lower than the Bohm speed throughout the entire domain ( $u/u_0 < 1$ ) but, in presence of collisions, the Bohm criterion has to be revised. We refer to other works for a more detailed discussion.<sup>2</sup>

Even though the overall agreement is satisfying we believe this distance between the models can be reduced increasing furthermore the pressure in the discharge; unfortunately the computational cost of all the approaches presented here increases dramatically as we approach the limit  $Kn_{kn} \rightarrow 0$ : such phenomena is a well-known problem of this type of equations.<sup>14</sup>

A general remark on the different multicomponent approaches: both the binary diffusion and the multicomponent diffusion simulations show similar behaviour (even though the mismatch is much more evident at lower pressure) even though the numerical discretization is different between the two. This was an aspect predicted in the modeling section (Sec.2.2) and proves the quality of the implementation of the methods.

## MULTICOMPONENT FLUID SOLVER FOR ARGON PLASMA

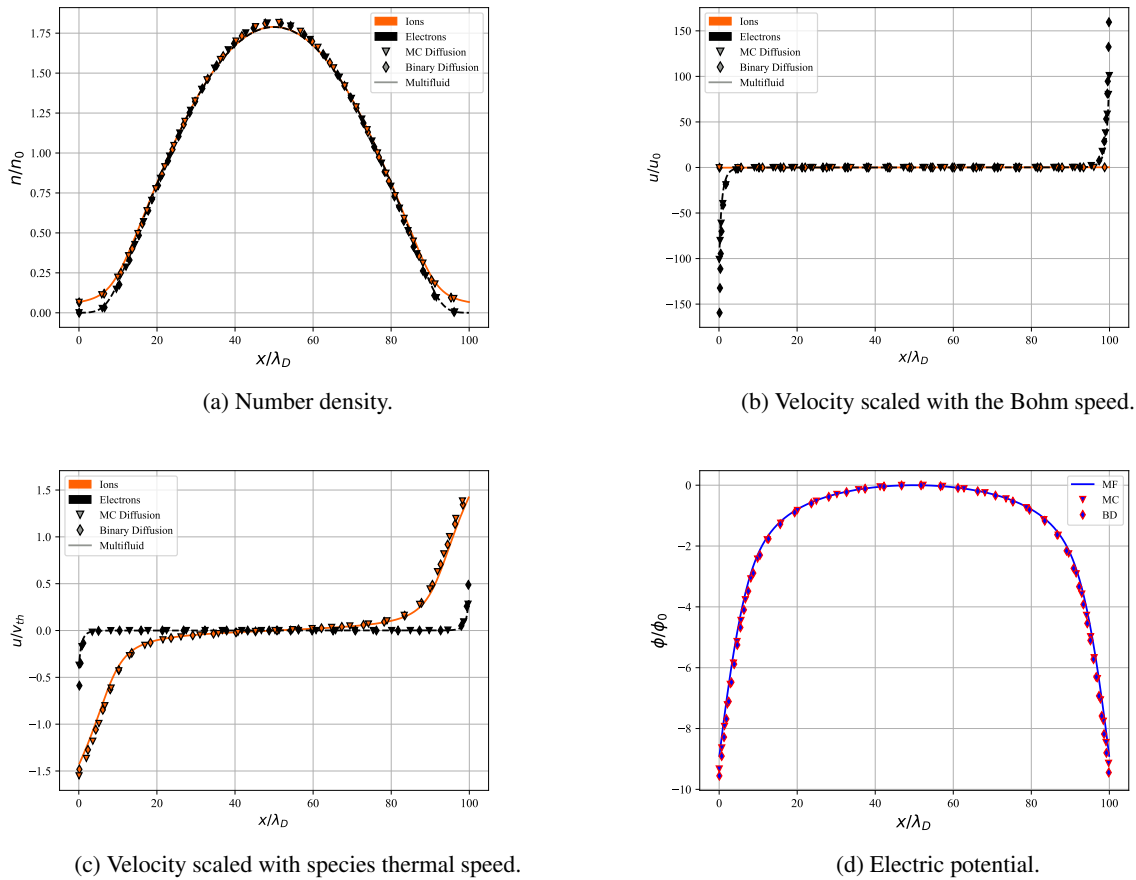


Figure 6: High pressure (1000 Pa) solution for the multifluid, binary diffusion and multicomponent diffusion models.

## 5. Conclusions

We presented here the development of a multicomponent fluid solver for a two-temperatures argon plasma: we applied the developed tool to the problem of plasma-sheath formation comparing the proposed multicomponent diffusion approach, based on a rigorous kinetic derivation from the Boltzmann equation, to the multifluid model, widely used in the plasma physics, for a wide range of pressures.

The three presented approaches agree well in highly collisional regimes, with this agreement decreasing when the number of collisions decreases: lowering the pressure, the models become progressively more distant from the purely diffusive limit, which was at the base of the multicomponent philosophy used in this work; such behaviour suggests that this assumption must be revised and will be the object of upcoming new developments.

A detailed analysis of the computational cost of the models presented is left for future works: nevertheless it is clear that the implicit (or semi-implicit) treatment of the diffusive terms in the proposed multicomponent approaches allowed to obtain satisfying results in a very stiff problem; however, as already discussed, our formulation suffers of the typical increase in computational cost that other works discussed in slightly different frameworks; asymptotic preserving strategies are under investigation and will be the object of future works.

Despite the numerical challenges that the problem presented, results obtained are satisfying allowing to focus in the future both on treating more complex mixture (like air plasmas), removing the isothermal assumption and adding accurate description of the chemistry, and to the development of valid numerical schemes suited to overcome the numerical challenges that have been widely discussed in the present document.

## 6. Acknowledgements

The first author is financed by the Fonds National de Recherche Scientifique (FNRS) through the FRIA grant.

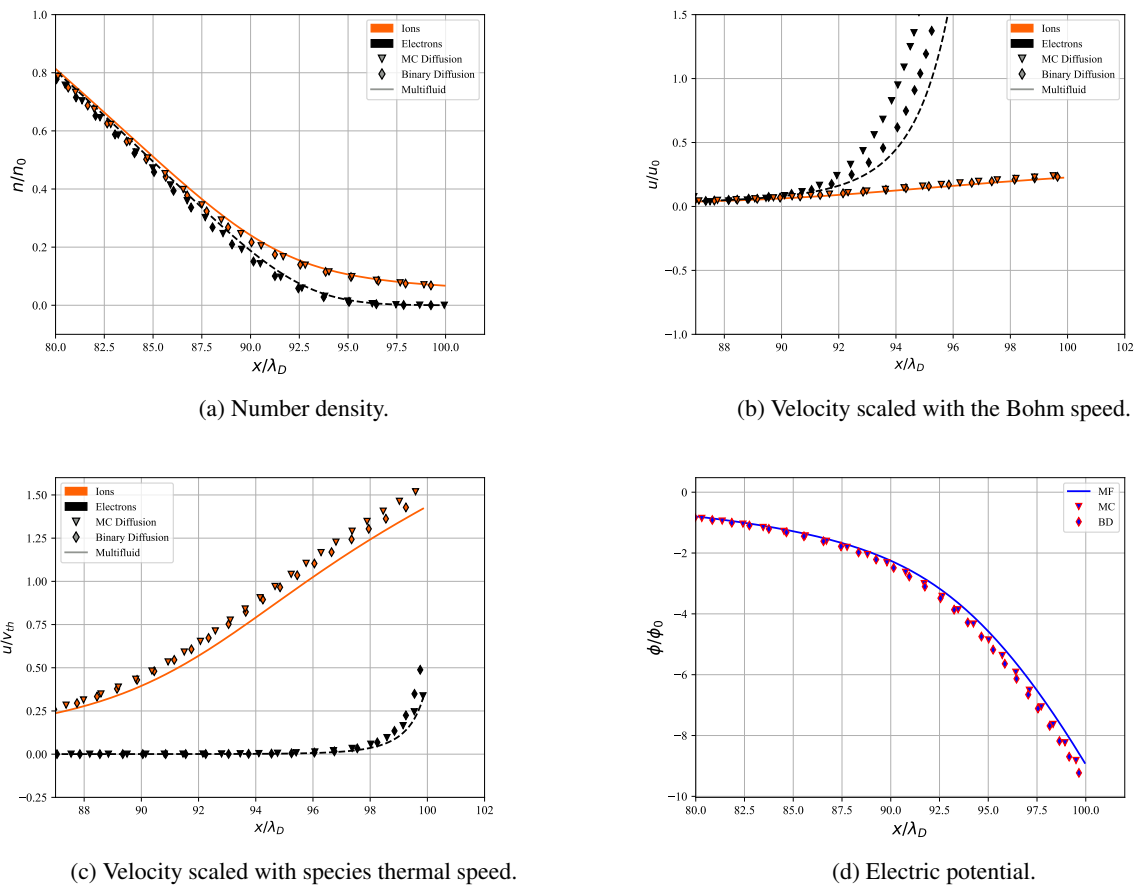


Figure 7: High pressure (1000 Pa) solution for the multifluid, binary diffusion and multicomponent diffusion models (Particular of the sheath region).

## References

- [1] Alejandro Alvarez Laguna, Andrea Lani, Yana Maneva, Herman Deconinck, and Stefaan Poedts. Computational multi-fluid model for partially ionized and magnetized plasma. In *47th AIAA Plasmadynamics and Lasers Conference*. American Institute of Aeronautics and Astronautics, 2016.
- [2] Alejandro Alvarez Laguna, Thierry E. Magin, Marc Massot, Anne Bourdon, and Pascal Chabert. Plasma-sheath transition in multi-fluid models with inertial terms under low pressure conditions: Comparison with the classical and kinetic theory. *Plasma Sources Science and Technology*, 29(025003), 2020.
- [3] Alejandro Alvarez Laguna, Teddy Pichard, Thierry Magin, Pascal Chabert, Anne Bourdon, and Marc Massot. An asymptotic preserving well-balanced scheme for the isothermal fluid equations in low-temperature plasmas at low-pressure. *Journal of Computational Physics*, 419(109634):1–29, 2020.
- [4] Luis L. Alves and Annemie Bogaerts. Special issue on numerical modelling of low-temperature plasmas for various applications – part I: Review and tutorial papers on numerical modelling approaches. *Plasma Processes and Polymers*, 14(1690011):1–2, 2017.
- [5] Francisco J. Artola, Alberto Loarte, Ekaterina Matveeva, Josef Havlicek, Tomas Markovic, Jiri Adamek, Jordan Cavalier, Lukas Kripner, Guido T. A. Huijsmans, Michael Lehnen, Matthias Hoelzl, and Radomir Panek. Simulations of COMPASS vertical displacement events with a self-consistent model for halo currents including neutrals and sheath boundary conditions. *Plasma Physics and Controlled Fusion*, 63(6):064004, 2021.
- [6] Mikhail S. Benilov. A kinetic derivation of multifluid equations for multispecies nonequilibrium mixtures of reacting gases. *Physics of Plasmas*, 3(4):521–528, 1997.

## MULTICOMPONENT FLUID SOLVER FOR ARGON PLASMA

- [7] Marianne Bessemoulin-Chatard, Claire Chainais-Hillairet, and Marie-Hélène Vignal. Study of a finite volume scheme for the drift-diffusion system. asymptotic behavior in the quasi-neutral limit. *SIAM Journal on Numerical Analysis*, 52(4):1666–1691, 2014.
- [8] Annemie Bogaerts and Luis L. Alves. Special issue on numerical modelling of low-temperature plasmas for various applications – part II: Research papers on numerical modelling for various plasma applications. *Plasma Processes and Polymers*, 14(1790041):4–5, 2017.
- [9] Iain D. Boyd and Thomas E. Schwartzentruber. *Nonequilibrium Gas Dynamics and Molecular Simulation*. Cambridge Aerospace Series. Cambridge University Press, 2017.
- [10] Miroslav Čada and Manuel Torrilhon. Compact third-order limiter functions for finite volume methods. *Journal of Computational Physics*, 228(11):4118–4145, 2009.
- [11] Melvin R. Carruth, Jason A. Vaughn, Richard T. Bechtel, and P. A. Gray. Experimental studies on spacecraft arcing. *Journal of Spacecraft and Rockets*, 30(3):323–327, 1993.
- [12] Pascal Chabert and Nicholas Braithwaite. *Physics of Radio-Frequency Plasmas*. Cambridge University Press, 2011.
- [13] Pierre Degond, Alexei Lozinski, Jacek Narski, and Claudia Negulescu. An asymptotic-preserving method for highly anisotropic elliptic equations based on a micro–macro decomposition. *Journal of Computational Physics*, 231(7):2724–2740, 2012-04.
- [14] Giacomo Dimarco, Lorenzo Pareschi, and Giovanni Samaey. Asymptotic-preserving monte carlo methods for transport equations in the diffusive limit. *SIAM Journal on Scientific Computing*, 40(1):A504–A528, 2018.
- [15] Joel Henry Ferziger and Hans G. Kaper. *Mathematical Theory of Transport Processes in Gases*. American Elsevier Publishing Company, 1972.
- [16] L. Garrigues, B. Tezenas du Montcel, G. Fubiani, F. Bertomeu, F. Deluzet, and J. Narski. Application of sparse grid combination techniques to low temperature plasmas particle-in-cell simulations. i. capacitively coupled radio frequency discharges. *Journal of Applied Physics*, 129(15):153303, 2021.
- [17] Vincent Giovangigli. *Multicomponent Flow Modeling*. Birkhäuser, 1998.
- [18] Benjamin Graille, Thierry E. Magin, and Marc Massot. Kinetic theory of plasmas: Translational energy. *Mathematical Models and Methods in Applied Sciences*, 19(4):527–599, 2009.
- [19] Gerjan Hagelaar. Modelling methods for low-temperature plasmas. Technical report, Université Paul Sabatier, 2008.
- [20] Charles Hirsch. *Numerical Computation of Internal and External Flows*. Fundamentals of Computational Fluid Dynamics. Elsevier, second edition edition, 2007.
- [21] Thierry E. Magin and Gérard Degrez. Transport algorithms for partially ionized and unmagnetized plasmas. *Journal of Computational Physics*, 198(2):424–449, 2004-08-10.
- [22] Thierry E. Magin and Gérard Degrez. Transport properties of partially ionized and unmagnetized plasmas. *Physical Review E*, 70(4):046412, 2004-10-28. Publisher: American Physical Society.
- [23] Alessandro Munafò. *Multi-Scale models and computational methods for aerothermodynamics*. phdthesis, Ecole Centrale Paris, 2014. Issue: 2014ECAP0008.
- [24] John D. Ramshaw and C. H. Chang. Ambipolar diffusion in two-temperature multicomponent plasmas. *Plasma Chemistry and Plasma Processing*, 13(3):489–498, 1993.
- [25] Karl U. Riemann, Josef Seebacher, Davy D. Tskhakaya Sr, and Siegbert Kuhn. The plasma–sheath matching problem. *Plasma Physics and Controlled Fusion*, 47(11):1949–1970, 2005.
- [26] James B. Scoggins, Vincent Leroy, Georgios Bellas-Chatzigeorgis, Bruno Dias, and Thierry E. Magin. Mutation++: MULTicomponent thermodynamic and transport properties for IONized gases in c++. *SoftwareX*, 12:100575, 2020.

MULTICOMPONENT FLUID SOLVER FOR ARGON PLASMA

- [27] Luke Uribarri and Edward H. Allen. Electron transpiration cooling for hot aerospace surfaces. In *20th AIAA International Space Planes and Hypersonic Systems and Technologies Conference*, International Space Planes and Hypersonic Systems and Technologies Conferences. American Institute of Aeronautics and Astronautics, 2015.
- [28] Vladimir Zhdanov. *Transport Processes in Multicomponent Plasma*, volume 44. Taylor & Francis, 2002.